Super-relativistic fluxon in a Josephson multilayer: Experiment and simulation

J. Zitzmann* and A. V. Ustinov
Physikalisches Institut III, Universität Erlangen, D-91058 Erlangen, Germany

M. Levitchev†
Institut für Schicht- und Grenzflächenforschung, Forschungszentrum Jülich, D-52425 Jülich, Germany

S. Sakai
Nanoelectronics Research Institute, National Institute of Advanced Industrial Science and Technology, 1-1-4 Umezono, Tsukuba-shi, Ibaraki 305, Japan

(Received 26 April 2002; published 29 August 2002)

The propagation of a single Josephson vortex is studied experimentally in stacks of five and ten Nb-Al/AlO_x-Nb annular Josephson tunnel junctions. To gain a detailed insight in the dynamics of the system, experimental data are compared to numerical simulations. This comparison enables us to determine the particular junction in the stack in which the vortex is located. We study in detail the interaction of the vortex with the Josephson plasma oscillations at different temperatures that correspond to different dissipation values. At low temperatures, the resonant locking of the vortex to the emitted Cherenkov waves is observed. At high temperatures, the nonresonant behavior of the vortex is found. Experimental data, simulation, and analytical models are in good agreement, and show a consistent picture of the dynamics of a single vortex in the stack.

DOI: 10.1103/PhysRevB.66.064527 PACS number(s): 74.50.+r, 74.80.Dm, 85.25.Dq, 41.60.Bq,

I. INTRODUCTION

Kleiner and Müller's finding of the intrinsic Josephson effect in highly anisotropic high-T_c superconductors[1] gave a strong impetus to the research in the field of Josephson physics. Anisotropic high-T_c superconductors are in essence vertical stacks of Josephson junctions produced by nature. Due to the close spacing of the superconductor-insulator lattice, the superconducting screening currents range across many layers and induce a coupling between the individual junctions. The dynamics of magnetic flux quanta in Josephson junction multilayers has raised a lot of interest for they are good candidates for high power flux-flow oscillators at THz frequencies, as shown in simulations.[2–4] Yet the predicted in-phase mode is still to be confirmed experimentally.

To investigate the mechanisms that govern the fluxon dynamics in high-T_c multilayers we mimic them by artificial stacking of Nb-Al/AlO_x-Nb junctions.[5] This approach allows us to control the sample properties in a wide parameter range, and the samples can be tailored for experimental and application purposes. Nb-Al/AlO_x-Nb stacks with as many as 28 junction layers have been produced,[6] with a typical spread of the critical currents of less than 10%. This makes the low-T_c systems an interesting counterpart to high-T_c mesa structures, where the achievable number of junctions ranges between a few and several hundred. Besides modeling intrinsic Josephson junctions, Nb-based stacks also provide a high integration level for cryoelectronic chips. Regarding possible applications as flux-flow oscillators, the fluxon dynamics is the most interesting field to investigate in stacks with a large number of junctions N.

It is very important to learn about *the simplest dynamic states* in stacks before moving into the very complex multivortex flux-flow regime. This regime differs greatly from its counterpart found in single-junction flux-flow oscillators. Therefore, our primary objective here is to study and understand the dynamics of *a single Josephson vortex* in the $(\text{Nb-Al/AlO}_x)_N$-Nb system. Yet despite the obvious attractiveness of high-N systems, the only experimental studies of single Josephson vortices done until now were using twofold stacks.[7,8] The underdamped single-vortex propagation in stacks with the number of junctions larger than two has been analyzed and studied numerically in Refs. 3 and 9–11, but no experiments have been made until now. The central message of this paper is reporting such experiments for the first time, to the best of our knowledge.

A single vortex in an underdamped junction stack may exceed the lowest characteristic velocity of Josephson plasma waves. In this case the vortex does not behave as a *relativistic particle* of solitonic nature as it does in single Josephson junctions, but its motion becomes *super-relativistic* (it overcomes the characteristic electromagnetic wave velocity) and is accompanied by Cherenkov radiation of Josephson plasma waves.[7] Experimental and numerical results show that in twofold stacks only one out of the two linear modes can be excited. In higher-order systems, however, N of these modes[12,5] exist and may affect the fluxon dynamics. In measurements presented below we were able observe such dynamics in a multilayer Josephson media with 5–10 junctions. To interpret the data and ultimately determine the excited plasma modes, we perform numerical simulations using the inductively coupled Josephson junction model.

The paper is organized as follows. In Sec. II we review the model which describes the dynamics of the phase differences in stacks and discuss linear modes. The experimental results are presented and compared with the simulations in Sec. III. Particular dynamic regimes at various temperatures are discussed here in detail. Section IV concludes the work.

II. THEORETICAL MODEL

An N-fold stack of long Josephson junctions, consisting of N insulating and $N+1$ superconducting layers (see Fig.

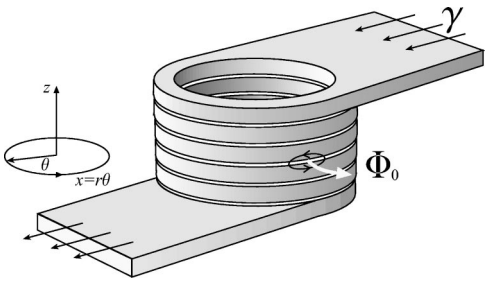

FIG. 1. Geometry of the annular Josephson junction stack of $N=5$ junctions; a fluxon is accelerated clockwise under the influence of the (normalized) bias current $\gamma=I/J$.

1), is well described by the Sakai-Bodin-Pedersen model of coupled sine-Gordon equations.[13] The equations which govern the phase dynamics in the Josephson stack are written as

$$\frac{\hbar}{2e\mu_0}\partial_{xx}\phi_l = s_{l-1}j^z_{l-1} + d'_l j^z_l + s_l j^z_{l+1}, \tag{1}$$

where $l=1\ldots N-1$, and

$$j^z_l = \frac{\hbar}{2e}C_l\partial_{tt}\phi_l + \frac{\hbar}{2e}G_l\partial_t\phi_l + J_l\sin\phi_l - I_l$$

is the total current flowing through junction l in the z direction. Here C_l, G_l, J_l, and I_l denote the unit area capacitance, conductance, critical current, and bias current, respectively. We assume that the junctions are connected in series and, therefore, receive the same bias current $I_l=I$ for all l. The parameters $G_l=G$ and $C_l=C$ are taken equal for all layers. The effective junction thickness d'_l and the coupling parameter s_l are defined in Ref. 13.

Neglecting the quasiparticle damping and inserting an ansatz of linear traveling waves $\phi_l=A_l\exp[i(kx-\omega t)]$ with small amplitude into Eqs. (1) yields the dispersion relation of the eigenmodes:

$$\omega_m^2 = \omega_p^2 + (c_m^{(N)})^2k^2 \quad \text{with} \quad m=1,\ldots,N. \tag{2}$$

The values $c_m^{(N)}$ are called characteristic velocities, and can be calculated[5] by solving the eigenvalue problem of the coupling matrix from Eq. (1). Note that, unlike in single long junctions, the maximum velocity of fluxons in stacks is generally unknown[9] and does not necessarily coincide with the minimum phase velocity of linear waves $c_N^{(N)}$. In particular, fluxon motion at velocities higher than $c_N^{(N)}$ is possible and it leads to excitation of traveling plasma waves by the fluxon.[7]

Since an analytical treatment of Eq. (1) is hardly possible, numerical simulations prove to be the most valuable tool for gaining insight into the dynamics of Josephson junction stacks. The numerical procedure that we employ for solving Eqs. (1) is based on the finite difference scheme described in Ref. 14. To check the accuracy of the algorithm, we have compared our results with those of a simulation routine by Kleiner *et al.*,[3] which applies a Fourier expansion method to solve Eqs. (1). Good agreement between the results of both algorithms has been found.[10]

III. RESULTS AND DISCUSSION

Single-vortex states have been prepared and measured in ring-shaped stacks of $N=5$ and 10 junctions; see Fig.1. In order to exclude the influence of the junction edges and study of the vortex motion under periodic boundary conditions we used the annular junction geometry. The circumference L of 418 and 597 μm (cf. Table I) of the samples was large compared to the typical Josephson length. The thicknesses of the superconducting Nb films were comparable to the London penetration depth $\lambda_L\approx 90$ nm at $T=0$ K, so that strong inductive coupling was achieved between the junctions.

To induce a Josephson vortex into the system, the samples are cooled through the critical temperature $T_c=9.2$K while a small bias current is applied. Below T_c the number of vortices trapped in the junctions is conserved due to the magnetic flux quantization and the topology of the sample. Since trapping of vortices in Josephson multilayers turns out to be considerably more difficult than in single junctions, great care is taken to determine the resulting state. The number of freely moving vortices in the stack is determined from the maximum voltage of the fluxon step obtained from a measurement of the current-voltage characteristic (CVC). Furthermore, the critical current diffraction pattern is measured (see Fig. 2) to check the obtained state.[15,7] This method is also a sensitive probe for the possible pinning of the vortex by defects or parasitic flux in the films.

TABLE I. Properties and parameters of the measured samples.

Sample	Layers N	Length (μm)	Thicknesses of the Nb films (nm)			Critical current density at 4.2 K (A/cm^2) [a]
			top	intermediate	bottom	
1	5	416	180	90	90	90
2	5	416	180	90	90	130
3	5	416	180	90	90	140
4	5	597	180	90	90	140
5	10	416	120	60	90	81
6	10	597	120	60	90	81

[a]The spread of the critical current density in all samples is below 5%, except for sample No. 1, where one of the junctions has a critical current density of 145 A/cm^2.

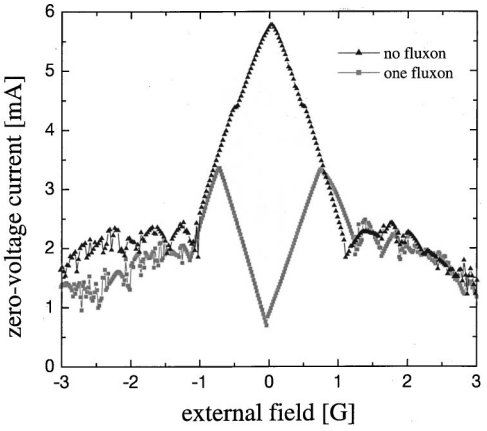

FIG. 2. The critical current diffraction patterns for sample No. 2 measured for the fluxon-free state and with a fluxon trapped in one of the junctions.

Since the quasiparticle tunneling conductance G decreases exponentially with temperature, the damping in the system is controlled by varying the temperature between 1.3 and 9.2 K. A typical set of measurements is shown in Fig.3. Note that at low temperatures we find resonances on the fluxon CVC, which vanish as the temperature is increased. Close to T_c the fluxon step does not approach any asymptotic voltage as found in single junctions, but instead shows an S shape. In the following sections, the fluxon dynamics in the low and high temperature regimes is analyzed with the help of numerical simulations of Eqs. (1).

A. Low damping regime

At low temperature the damping due to the quasiparticle tunneling is sufficiently small so that Josephson plasma waves have significant influence on the dynamics of the fluxons. Due to the periodic boundary conditions in the annular junctions, there exist only eigenmodes (2), with wave numbers $k_h=(2\pi/L)h$, exist, where $h=1,2,\ldots,\infty$. These plasma waves can be excited when the Cherenkov condition holds, i.e., the fluxon velocity v_{fluxon} equals the phase velocity of linear waves $v_{\text{phase}}=\omega/k$.

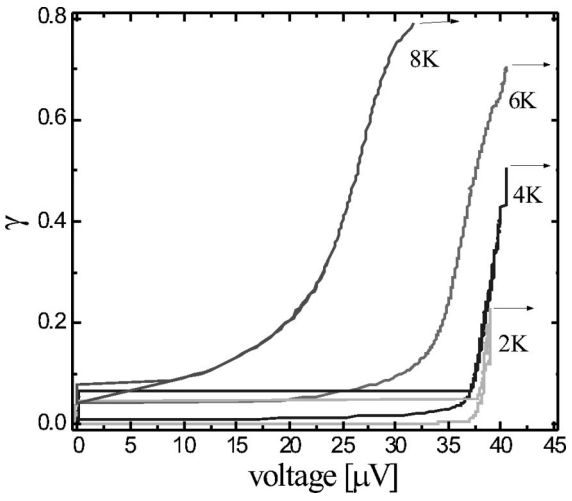

FIG. 3. Measured CVC's of a single fluxon in the center barrier of sample No. 3. The labels on the curves indicate the temperature; γ is the bias current normalized to the fluxon-free critical current of the stack.

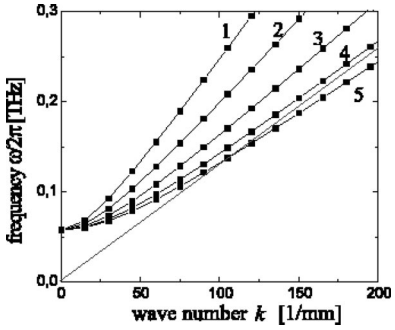

FIG. 4. Plasma dispersion relation calculated for the fivefold stack No. 3. The numbers indicate the dispersion branch m; squares correspond to the resonant modes counted by index h; the straight line illustrates the fluxon velocity v_{fluxon}.

Using the dispersion relation for linear plasma waves [Eq. (2)], one finds that Cherenkov modes are excited at a fluxon velocity of[7]

$$v_{\text{res}}=\sqrt{(c_m^{(N)})^2+\left(\frac{\omega_p L}{2\pi h}\right)^2}. \tag{3}$$

From Eq. (2) it is clear that the lowest characteristic velocity $c_N^{(N)}$ plays the role of a lower bound of the fluxon velocities at which Cherenkov radiation exists (see Fig. 4).

To test whether this prediction is correct, the phase dynamics of a single fluxon in the center junction of sample No. 3 at 4.2 K is simulated. The junction parameters are either known from the sample fabrication (dimensions), single-junction measurement data (capacitance $C=3.2\mu\text{F}/cm^2$) or are obtained by direct measurements (e.g., the critical current $J=140$ A/cm^2). The tunnel conductance can be deduced from the nonrelativistic part of the CVC. For all simulations the dependence of the parameters such as damping in Eq. (1) on temperature is taken into account, while a stochastic term to simulate fluctuations was not taken into account. For numerical analysis a conductance $G=60$ kS/cm^2 of about twice the real value at $T=4.2$ K is used. Such an increased conductance corresponding to higher damping was chosen in order to reduce the computation time. For this reason we also refrained from a detailed analysis of data obtained at temperatures lower than 4.2 K. Figure 5 shows the calculated CVC of a fluxon captured in the center junction No. 3 of the stack at 4.2 K. This junction is referenced by $l=3$ in Eq. (1). The corresponding profiles of the sine of the phase differences at the bias points labeled in roman are plotted in Fig. 6. The vertical lines with Arabic labels in the inset of Fig. 5 correspond to the analytically calculated resonant velocities [Eq. (3)] and demonstrate excellent agreement with the results of simulation.

With the aid of the simulated phase differences it is now possible to understand the dynamics of the fluxon in the stack. At fluxon velocities smaller than the lowest characteristic velocity $c_5^{(5)}$ in Fig. 6i, one can identify the fluxon in the

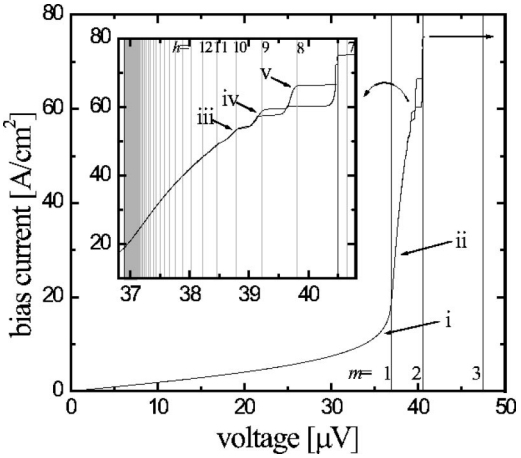

FIG. 5. Simulated CVC of a single fluxon in the center barrier using the parameter set for sample No. 3 at 4.2K. Vertical lines in the main plot indicate the characteristic velocities $c_m^{(N)}$; the vertical lines in the inset show the voltages corresponding to the resonant velocities v_{res} of the mode h.

center junction and its images in the other junctions. When v_{fluxon} exceeds $c_5^{(5)}$, an oscillating tail of Cherenkov radiation arises behind the fluxon. Figure 6*ii* shows that the amplitude of these waves quickly decays in space and time due to the damping. With increasing velocity, the fluxon excites modes with lower h and larger wavelength. In addition, the amplitude of the Cherenkov wake, and therefore its length, grow. Once the Cherenkov wake extends over the circumference of the junction, the fluxon interacts with its radiation and v_{fluxon} locks to v_{res}. Intuitively thinking, one may say that the fluxon is trapped in the potential created by its wave tail and can overcome v_{res} only if the driving force γ exceeds the force due to this potential. Therefore, the velocity v_{fluxon} locks to discrete values and hysteretic resonant steps appear on the CVC. These in turn can be assigned to the different wave numbers k_h of modes (2) as illustrated in Fig. 5. At even higher bias current, the amplitude of the plasma waves exceeds 2π in the junction where the fluxon is located. This results in the creation of a fluxon-antifluxon pair in this junction. The Lorenz force due to the bias current pulls the created fluxon and antifluxon in opposite directions. An instant later, the pair causes the nucleation of further fluxons and antifluxons in all other junctions and this avalanche switches the stack to the phase-whirling state.

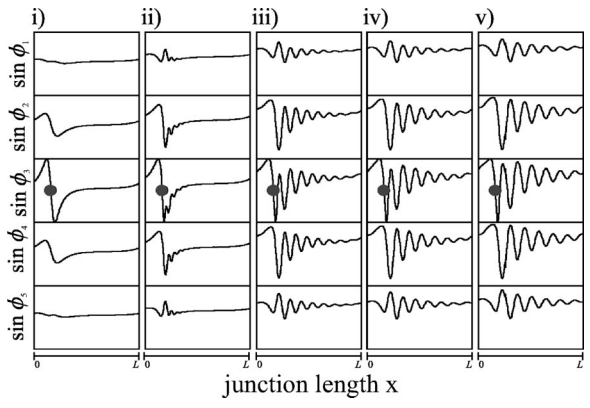

FIG. 6. The simulated profiles of $\sin\phi_l$ in sample No. 3 with a fluxon in the center barrier for the bias points indicated in Fig. 5: $\gamma_{(i)}=0.07$, $\gamma_{(ii)}=0.22$, $\gamma_{(iii)}=0.38$, $\gamma_{(iv)}=0.42$, and $\gamma_{(v)}=0.47$. The fluxon is marked by a circle.

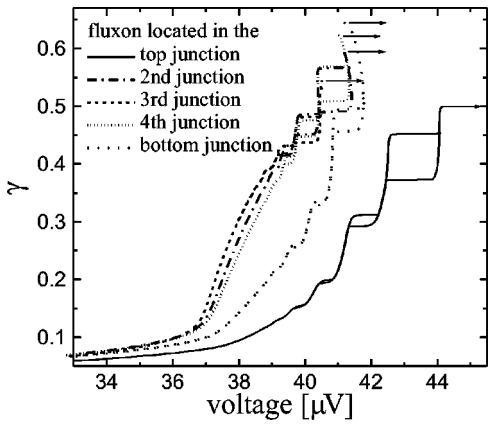

FIG. 7. High-velocity range of simulated CVC's for all five possible single-fluxon states in sample No. 3. The different curves correspond to fluxon located in different junctions.

But simulation can do more than giving insight in the phase dynamics. Looking at the experimental CVC of a single fluxon state, it is not known *a priori* in which junction out of the N junctions of the stack the fluxon is trapped. Nevertheless, by comparing the measured data with the simulations we can approximately determine the junction in which the fluxon is located. This can be decided from the features of the relativistic part of the CVC, such as its shape and curvature, as well as from the positions of the resonances and their switching currents. The CVC's for all possible single-fluxon states simulated with the parameter set of stack No. 3 are presented in Fig. 7. The fluxon state characteristics are distinct for the top and bottom junctions, because they both are lacking a neighboring junction on one of their sides. The distinction between the bottom and top junctions themselves is due to the difference in thickness of the top and

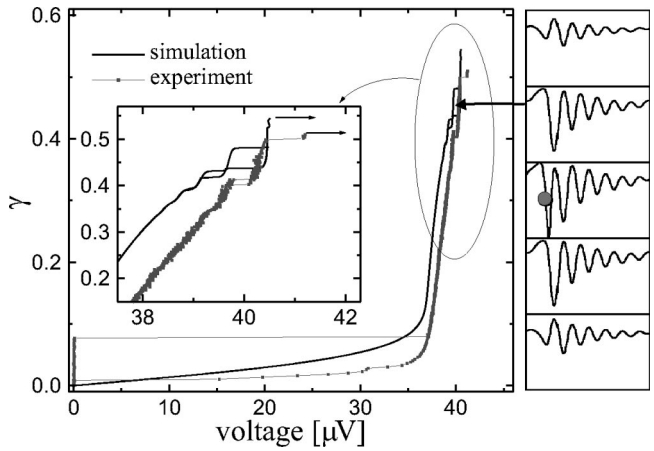

FIG. 8. Measured and simulated CVC's of a single fluxon in the center junction of sample No. 3 at 4.2 K. The onset shows the simulated profiles of the phase differences at the marked point.

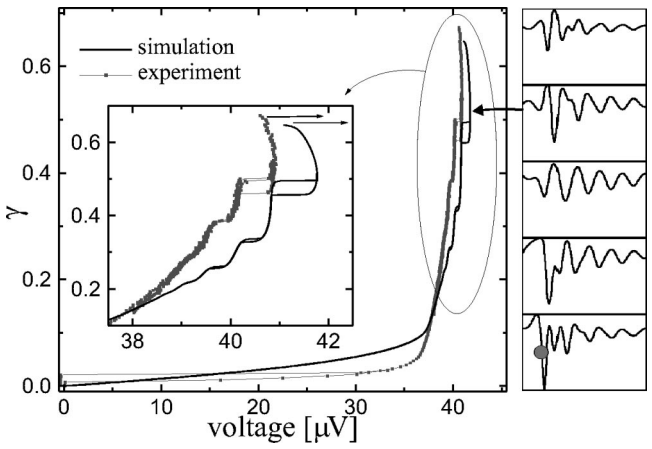

FIG. 9. Measured and simulated CVC's of a single fluxon in the bottom junction of sample No. 3 at 4.2 K. The onset shows the simulated profiles of the phase differences at the marked point. Note the negative differential resistance on the top of the upper step.

bottom Nb film (see Table I). Still, states with fluxon in inner junctions cannot be sorted and identified with sufficiently good confidence.

The experimental data in Figs. 8 and 9 show two different single fluxon states in sample No. 3. The differences in the measured CVC's enable us to conclude that for Fig. 8 the fluxon is located in one of the inner junctions, while for Fig. 9 it is trapped in the bottom junction. Cycling the sample through T_c allows us to catch various fluxon states, which can easily be identified by their respectively reproduced CVC's. The disagreement between the simulated and measured CVC's is mainly due to the sensitive dependence of the data on variations in the tunnel conductances G_l in the junctions.

Note that the CVC's in Figs. 8 and 9 cross over the voltage value corresponding to $c_4^{(5)}$. Thus linear Josephson plasma modes can be excited on the $m=4$ and 5 branches of the dispersion relation, which is illustrated by the profile of the phase differences in the inset of Fig. 9. This clearly poses the question on the maximum velocity of the fluxon in the stack, which so far is still not fully solved theoretically[9] for stacks with arbitrary N. When the fluxon is located in the bottom junction, we note the negative differential resistance at the top of the fluxon step in both measurements and simulation. A qualitative explanation for this feature is given in Sec. III D.

Experiments also show that at lower temperature the jump to the gap occurs at a considerably lower bias current than at higher temperature (see Fig. 3). As mentioned above, simulations prove that the switching to the resistive state is due to the creation of a fluxon antifluxon avalanche in the fluxon tail. In this process, the amplitude of Cherenkov oscillations in the tail needs to exceed 2π, which in systems with lower damping happens at a lower bias current. Understanding the energy distribution between the fluxon and its radiation might lead to a theoretical model for the switching currents.

B. Crossover between the low and high damping regimes

As mentioned above, an increase in temperature drastically raises the quasiparticle tunneling and, therefore, the

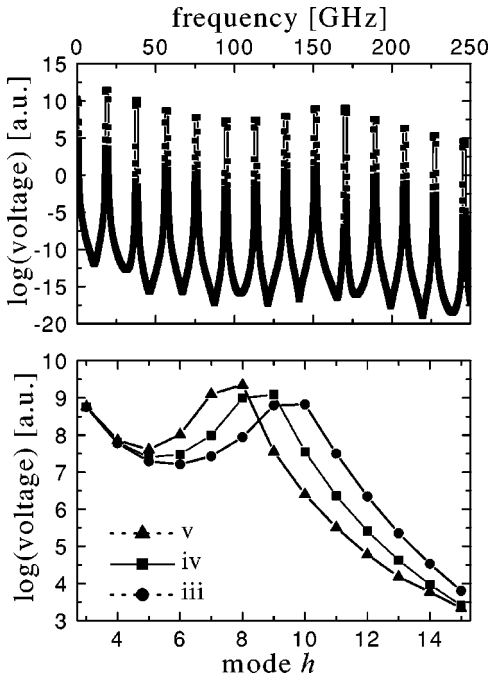

FIG. 10. Top: Spectral analysis of the voltage in a annular fivefold stack at the resonance (iv) of Fig. 5. Bottom: Harmonic amplitudes for the resonances (iii), (iv), and (v) from Fig. 5.

damping in the stack. The Cherenkov oscillations induced by a moving fluxon are damped by the increased quasiparticle conductance G. In consequence, the decay length of the oscillating tail created by the fluxon decreases and the resonances on the fluxon step cease to exist (cf. Fig. 3). Yet because of its topologically solitonic nature, the fluxon state preserves.

Another general effect associated with the damping in the Cherenkov tail is the broadening of the radiation line width. In particular, for the Josephson stack, quickly decaying wave tails do not lock to the sample cavity modes anymore, so that a broader spectrum of waves can be excited. To gain insight into the nature of the broadening of the linear mode frequencies, we performed a spectral analysis of the numerically simulated voltages in the stack. The parameters for the simulations were again chosen to match the characteristics of sample No. 3 at 4.2 K. To determine the Cherenkov mode h that is excited at resonances (iii)–(v) in Fig. 5, a Fourier transform of the voltage across the stack at an arbitrary chosen spatial point is evaluated. The spectrum of the sampled data at $\gamma_{(iv)}=0.42$ in the top plot of Fig. 10 corresponds to a periodic set of harmonics. The voltage in the time domain will always peak when the fluxon, and its images pass by the sampling point. The fundamental Josephson frequency of 18.9 GHz is associated with the fluxon rotation, and its higher harmonics form a frequency comb. The relatively large power of the high harmonics is due to the sharpness of the fluxon pulse in the time domain, which is caused by its spatial contraction.

Knowing that at zero damping the fluxon velocity locks to v_{res}, the radiation emitted from mode h adds to the hth fluxon harmonic. When the plasma spectrum is broadened by dissipation, the plasma radiation power is overlaying the

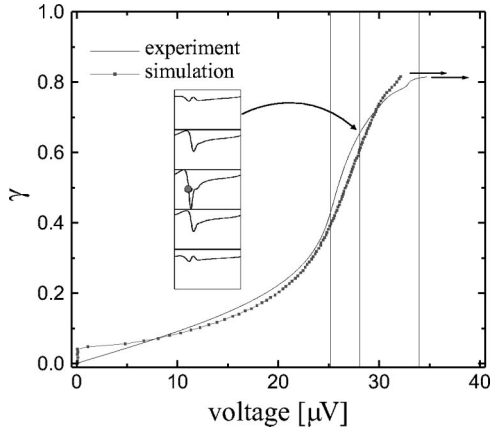

FIG. 11. Measured and simulated CVC's of a single fluxon in the center junction of sample No. 3 at 8 K. The inset shows the profile of the phase differences at the marked point. The vertical lines indicate characteristic velocities $c_5^{(5)}$, $c_4^{(5)}$, and $c_3^{(5)}$.

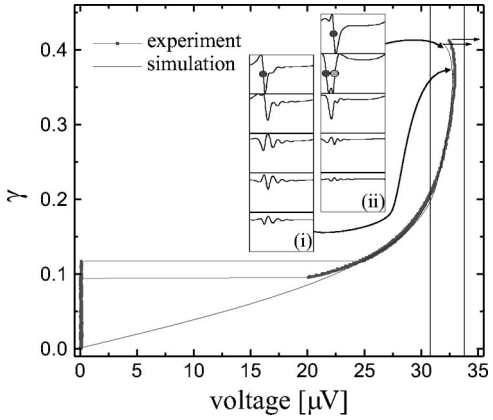

FIG. 12. Measured and simulated CVC's of a single fluxon in the strong junction of sample No. 1 at 6.8 K. The profiles of the phase differences are shown as insets for the bias points $\gamma_{(i)} = 0.38$ and $\gamma_{(iv)} = 0.412$. The vertical lines indicate characteristic velocities $c_5^{(5)}$ and $c_4^{(5)}$.

fluxon frequency comb. The top graph of Fig. 10 shows the spectrum of bias point (iv) in Fig. 5. We find a rise in the amplitude of the harmonics ranging from approximately 130–200 GHz. The rise in Fourier amplitude due to the plasma waves is much smaller than the fluxon harmonics amplitudes. To determine which modes are excited at the resonances indicated by (iii), (iv), and (v) in Fig. 5, the local maxima of the Fourier spectrum are shown in the bottom plot of Fig. 10 (data binning was applied to ensure that the variance of the Fourier amplitudes is much smaller than the amplitudes themselves). Our results are in agreement with that of Ref. 11, showing that multiple Cherenkov modes can be excited by fluxon at a time. We find that the resonance significantly broadens over several modes already at quite low damping. The exited mode numbers $h=8$, 9, and 10 from the simulation nicely coincide with the analytical prediction plotted in Fig. 5.

C. High damping regime

Rising the temperature of the sample with the fluxon state shown in Fig. 8 from 4.2 to 8 K, the quasiparticle conductance increases to about $G=174$ kS/cm^2. Due to this increased damping the Cherenkov radiation behind the fluxon quickly decays and the resonances on the CVC vanish, as can be seen in Fig. 11. Yet the velocity of the fluxon does not asymptotically saturate at some value as observed for solitons in single junctions. In contrast, an S shape of the CVC is clearly observed in experiment and numerical simulation. Similarly, at 8 K the fluxon state of Fig. 9 shows an S-shaped CVC in both measurements and simulation (not shown). This is remarkable considering that the CVC of this state at 4.2 K shows a negative differential resistance just below the switching current.

The absence of a limiting velocity for a fluxon in a stack indicates that the fluxon lacks the properties of a relativistic soliton. Yet the fluxon maintains its topological stability, as indicated by numerical simulations. The ballistic propagation of solitons known for single-layer Josephson transmission lines is not found for fast fluxons in stacks. In addition to dissipative losses, the fluxon in a stack loses its energy due to Cherenkov radiation of Josephson plasma waves.

We would like to note that similar S-shaped characteristics have also been observed for flux-flow states in high-T_c intrinsic BiSrCaCuO Josephson junction stacks.[16] In that data the number of moving fluxons is very large, which strongly differers from our case here. The non-Josephson radiation observed by Hechtfischer *et al.*[16] was explained by Cherenkov emission and mixing between many Josephson plasma mode at close frequencies. This mechanism was supported by numerical simulations using the parameter set for intrinsic junctions.[17,18] Here we can only add that our observations on low-T_c stacks and numerical data for the high damping regime are consistent with the above works.

D. Back bending of resonances

As already mentioned in Sec. III A, we also observed negative differential resistance (back bending) on the top of the fluxon step. Such a behavior has been measured in sample No. 3 when the fluxon is located in the bottom junction (cf. Fig. 9). We find this effect to be even more pronounced in other samples, in particular in sample No. 1, as can be seen in Fig. 12. In this sample the critical current densities of the different junctions were not identical. Experimentally we find that one junction has a critical current density that is roughly 1.5 times higher than the others, specifically $J_5=145$ A/cm^2 and $J_{1,\ldots,4}=90$ A/cm^2 at 6.8 K. For the case of a twofold stack with nonidentical critical currents such a back bending was observed before.[8]

Through extensive simulations we found a sufficient (but not necessary) prerequisite to observe back bending. Considering the simulations shown in Fig. 6, this shows that the amplitude of the plasma waves is highest in the junction where the fluxon is located. Consequently the fluxon-antifluxon avalanche which leads to the rotating state will start in this junction. Clearly this holds for any stacked system with equal critical current densities of all junctions.

Simulations now show that for the case of sample No. 1 back bending will only occur if the fluxon is placed in the

junction with high critical current density, which we will call the strong junction. A look at the phase differences at the top of the fluxon step in Fig. 12 reveals different dynamics than the ones just discussed. As seen in the insets of Fig. 12, the fluxon is placed in the strong top ($l=5$) junction, and a damped wave tail originates from it. The image of the fluxon and its radiation is seen in the neighboring junctions. At the starting point of the back bending shown in inset (i), the phase difference in junction $l=4$ is just above $\pi/2$ (note that the plot shows $\sin\phi_l$ on the ordinate). As the bias current increases, so does the amplitude of the oscillation of the phase differences in this junction. When the amplitude exceeds 2π at $\gamma_{(iv)}=0.412$, a fluxon-antifluxon pair is created and the junction switches to the whirling state.

From this we can formulate a sufficient prerequisite for back bending. The phase difference in a junction not containing the fluxon has to be between $\pi/2$ and 2π. A practical test for this hypothesis are the data collected for sample No. 3. In fact, simulations show the same behavior as described above. A fluxon-antifluxon pair is created in the junction neighboring the junction with the fluxon. Clearly, back bending can now be identified as an effect based on the nonlinearity in the coupled sine-Gordon equations. As it is often seen in nonlinear systems, the dispersion of a traveling wave depends on its amplitude. It has been shown[19] that for long junctions a large amplitude of plasma waves leads to an effective reduction of their frequency. This reduction in frequency effectively decreases the phase velocity v_{phase} of the waves and, therefore, also the velocity v_{fluxon} of the fluxon that is locked to the resonance [Eq. (3)]. In the weak-coupling limit, this model is also applicable to stacks so that this mechanism qualitatively explains the back bending effect.

IV. CONCLUSION

We have studied the dynamics of single fluxons in fivefold and tenfold stacks of Josephson junctions experimentally and numerically. The resonances observed at low damping are well explained from the inductive coupling model as the effect of Cherenkov radiation of plasma waves. This mechanism governs the motion of the fluxon in the superrelativistic regime which extends above the lowest characteristic velocity of linear waves. In that range, the fluxon velocity may lock to the phase velocity of its radiation. Increased damping attenuates plasma waves and broadens their spectrum, so that a locking of the fluxon velocity to one of the modes is no longer possible. Nonetheless, the experimental evidence for the lack of the Lorenz invariance of the coupled sine-Gordon equations (1) is observed at high damping in the form of an S-shaped CVC. For low and intermediate damping, a back bending of the CVC is observed. It is attributed to the nonlinear resonance effect, in which the plasma wave frequency is reduced due to the large amplitude of the waves.

ACKNOWLEDGMENTS

We would like to acknowledge the help of N. Thyssen in the fabrication of the fivefold stacks. The authors are grateful to E. Goldobin, R. Kleiner, V. M. Krasnov, and B.A. Malomed for useful discussions. This work was supported by Deutsche Forschungsgemeinschaft (DFG).

*Present address: Institute of Physical Chemistry, ETH Hönggerberg, CH-8093 Zürich, Switzerland.

†Present address: Institut for Physics of Microstructures RAS, GSP-105, 603600 Nizhny Novgorod, Russia.

[1] R. Kleiner, F. Steinmeyer, G. Kunkel, and P. Müller, Phys. Rev. Lett. **68**, 2394 (1992); R. Kleiner and P. Müller, Phys. Rev. B **49**, 1327 (1994).

[2] A. V. Ustinov and S. Sakai, Appl. Phys. Lett. **73**, 686 (1998).

[3] R. Kleiner, T. Gaber, and G. Hechtfischer, Phys. Rev. B **62**, 4086 (2000).

[4] M. Machida, T. Kozama, A. Tanaka, and M. Tachiki, Physica C **330**, 85 (2000).

[5] S. Sakai, A. V. Ustinov, H. Kohlstedt, A. Petraglia, and N. F. Pedersen, Phys. Rev. B **50**, 12 905 (1994).

[6] N. Thyssen, Ph.D. thesis, Forschungszentrum Jülich, Jülich, Germany, 1998.

[7] E. Goldobin, A. Wallraff, N. Thyssen, and A. V. Ustinov, Phys. Rev. B **57**, 130 (1998).

[8] E. Goldobin, A. Wallraff, and A. V. Ustinov, J. Low Temp. Phys. **119**, 589 (2000).

[9] E. Goldobin, B. Malomed, and A. V. Ustinov, Phys. Lett. A **266**, 76 (2000).

[10] J. Zitzmann, Master thesis, Universität Erlangen-Nürnberg, 2000, http://www.physik.uni-erlangen.de/pi3/ustinov/publications.

[11] V. M. Krasnov, Phys. Rev. B **63**, 064519 (2001).

[12] R. Kleiner, Phys. Rev. B **50**, 6919 (1994).

[13] S. Sakai, P. Bodin, and N. F. Pedersen, J. Appl. Phys. **73**, 2411 (1993).

[14] S. Sakai, A. V. Ustinov, N. Thyssen, and H. Kohlstedt, Phys. Rev. B **58**, 5777 (1998).

[15] S. Keil, T. Doderer, I. V. Vernik, A. Laub, H. Pressler, R. P. Huebener, N. Thyssen, A. V. Ustinov, and H. Kohlstedt, Phys. Rev. B **54**, 14 948 (1996).

[16] G. Hechtfischer, R. Kleiner, A. V. Ustinov, and P. Müller, Phys. Rev. Lett. **79**, 1365 (1997).

[17] G. Hechtfischer, R. Kleiner, A. V. Ustinov, and P. Müller, Appl. Supercond. **5**, 303 (1998).

[18] R. Kleiner, T. Gaber, and G. Hechtfischer, Physica C **362**, 29 (2001).

[19] A. V. Ustinov, B. Malomed, and E. Goldobin, Phys. Rev. B **60**, 1365 (1999).